Modeling optical fiber dynamics for increased efficiencies in scanning fiber applications

Eric J. Seibel[12], Christopher M. Brown[13], Matthew J. Kundrat[12], and Per G. Reinhall[2]

[1] Human Interface Technology Lab, College of Engineering, University of Washington, Seattle, WA 98195-2142 USA, (206) 543-5075, www.hitl.washington.edu
[2] Department of Mechanical Engineering, University of Washington, Seattle, WA, 98195-2600
[3] Department of Bioengineering, University of Washington, Seattle, WA, 98195

ABSTRACT

A cantilevered singlemode optical fiber is base-excited to create 2D amplitude-modulated resonant motion as a basis for a scanning fiber endoscope (SFE). Over the past few years, prototype SFEs have been developed with smaller sizes of the distal rigid tip which houses the fiber scanner. Our current prototype is 2 mm in diameter with 15 mm rigid length at the tip of a highly flexible shaft. A spiral scan pattern at 40 degrees field of view generates 250 rings (500 lines) at greater than 10 frames per second with negligible distortion at 10 micron resolution. Future SFEs will use microfabrication techniques to sculpt the optical fiber cantilever to form tapered and microlensed tips for the purpose of increasing field of view without increasing electrical power. Microfabrication of complex optical fiber geometries is guided by linear and nonlinear dynamic models of the resonant motion of these fiberoptic scanners. Linear finite element analysis (FEA) is used to match low amplitude motions of tapered and notched fiber geometries, indicating that more flexible regions or hinges can be designed into future fiber scanners for increased amplitude of motion without sacrificing frequency. Nonlinear models of the fiber dynamics are developed and the results help predict the more complex behavior of microfabricated fiber scanners at wider fields of view. Thus, sophisticated fiber dynamics models are used to guide the development of more efficient scanning fiber image acquisition sensors and systems, such as ultrathin flexible SFEs and low-cost sensors.

Keywords: endoscope, optical fiber, microfabrication, scanning, finite element analysis

INTRODUCTION

A scanning optical fiber system used for image acquisition and display offers several potential advantages over conventional instrumentation: microscale device size, high field of view and resolution capability, low-cost mass production of devices, and the capability to transmit high-quality and high-intensity light [1, 2]. Each of these attributes has the potential to be realized through the novel design of the resonant waveguide scanner. A fiber scanner functions by scanning a projected far-field light spot from the tip of a resonant waveguide. This light spot may be used to display a field of pixels or, if the backscattered light from this spot is detected, acquire an image of an illuminated object. Furthermore, the light may sense the local environment through evanescent optical interactions with indicator chemicals bound on the fiberoptic scanner. Using a fiber scanner as an image display device, light projected from the waveguide may be modulated in synchronization with waveguide actuation and focused onto an image plane one pixel at a time. The observer forms a stable image when the scanned pattern is repeated above the critical flicker rate for image fusion [3]. An image acquisition device functions in a similar manner to an image display device, projecting light from an actuated waveguide. However, instead of modulating the light source to form an image, backscattered light from the object is detected one pixel at a time. Optical fiber scanning has been demonstrated to be a viable approach to both image display [4] and acquisition applications [1, 2, 5].

Optical Fibers and Sensors for Medical Applications V, edited by Israel Gannot, Proceedings of SPIE Vol. 5691 (SPIE, Bellingham, WA, 2005) · 1605-7422/05/$15 · doi: 10.1117/12.592245

A scanning fiber device is dependent upon waveguide dynamics. Device design goals include: maximizing translational and angular tip displacement of the waveguide, designing the device to operate at resonant frequencies above the critical flicker rate for image fusion, and enabling the system to operate in a robust fashion generating a space-filling, repeatable scan with low base displacement. Geometry of the cantilevered waveguide scanner has a large impact on the dynamic response of the system, altering system resonant frequencies, and waveguide displacement. Thus, we hypothesize that selective mass distribution along the cantilevered fiber axis can improve scanner efficiency compared to an unmodified fiber.

Modifying the mass distribution of a commercial optical fiber is expected to vary the opto-mechanical properties of cantilevered fiber scanners driven at mechanical resonance. Tapering the free end of a fixed-free cantilever fiber has previously been shown to increase the vibration amplitude and deflection angle of a vibrating cantilever tip [6,7], an important finding since increasing tip deflection improves device performance, field of view (FOV), and electromechanical efficiency, while reducing scanner size. In this study, the response of a tapered cantilever structure with complex shape profile that provides large tip deflection at high resonance frequency was investigated both experimentally and theoretically using finite element analysis (FEA). In addition, custom microfabrication techniques that selectively remove the outer cladding material of the singlemode optical fiber were used to fabricate fiber scanners and corresponding FEA models. Once validated experimentally, the FEA model was used to predict scanner performance among various designs for the goal of improving fiber scanner efficiency. Although modeling linear fiber dynamics is limited to small fiber scanner FOV, the relative comparisons among fiber scanner designs for optimal efficiency is expected to be valid for all FOVs. This hypothesis is being tested by the use of finite difference solutions of the fiber dynamics that include one or more nonlinear terms of the equations of motion. Future comparisons of opto-mechanical fiber scanner designs will use models that account for the nonlinear dynamics which become significant at large base excitations resulting in wide FOVs.

METHODS

Methods - Numerical

Due to the complex geometry of the fiber we chose to carry out numeric modeling of the linear fiber dynamics using a commercial FEA program (ANSYS Inc., Canonsburg, PA). Experimentally determined damping constants, cantilever beam base excitation measurements, beam geometry data, and available material property information were used to construct the FEA model. The material properties of the fused SiO_2 cantilevered fiber scanner are density (2202 kg/m^3) and Modulus of Elasticity (73 GPa) for the singlemode optical fiber of 125 μm in diameter [8]. Beam cross-section measurements were acquired from photographs taken using a calibrated microscope. **Figure 1A** displays the measured radii of the beam along the axis of the beam, illustrating the complex tapered profile produced by the fiber heating and pulling method. Damping constants were measured experimentally for the first three modes of the tapered waveguide, and are listed in **Table 1**. The one-dimension (1D) base displacement amplitude that is input into the FEA model is 1 μm, a value representative of the base displacement experienced by the fiberoptic cantilevers at low levels of excitation. This analysis, based on Euler-Bernoulli beam theory is valid for these small base displacements only, where the fiber response is in the linear regime. The FEA model provides beam tip displacement and tip deflection angle information, allowing for the determination of centroid light spot location 2.5 mm from the free tip of the waveguide to match experimental conditions. Important modeling assumptions, in addition to the E-B beam theory assumption, include radial symmetry of the waveguide as well as isometric material properties following microfabrication.

Nonlinear fiber response is expected when the tip displacement is at the same order of magnitude as the diameter of the cantilevered beam (125 μm). Since linear FEA models cannot predict fiber dynamics at the desired wide FOVs, the nonlinear equations of motion of the fixed-free cantilever have been modeled and numerically solved for the simple cylindrical shape profile only. The nonlinear dynamics of a straight cylindrical cantilever beam of 10.2 mm long and 125 microns in diameter were analyzed numerically using a finite difference technique [9]. The equations of motion for a fixed-free, base-excited cantilever were

derived by Pai & Nayfeh [10]; however, our preliminary results include only the nonlinear bending term and not the nonlinear inertial term.

Methods - Experimental

Cantilever beam waveguides were made from commercial single-mode optical fiber (FS-SN-3224, 3M, Inc., St. Paul, MN). The outer buffer layer of the fiber was removed using a fiber-optic stripper (Micro-Strip, Klein Tool, Inc., Chicago, IL) and then adhered to a piezoelectric bimorph (600/200/0.6-SA, APC, Ltd., Mackeyville, PA). The original piezo bimorphs were machined to dimensions of approximately 2.0 X 5.0 mm with a rotary tool to decrease size and to increase the cut-off frequency response of the device. The waveguides were modified to a tapered geometry using a quartz fiber puller (Model P-2000, Sutter Instrument, Co., Novato, CA). In this device, lengths of optical fiber are heated with a CO_2 laser and pulled apart. Manipulation of settings on the micropipette pulling device - heat supplied by the laser output, overall heating, time and fiber pull rate - provide limited control over the geometry of the tapered waveguides. Using this device, variable length tapered optical fibers were formed, with tapered sections 1 - 4 mm in length with tip dimensions as small as 3 microns in diameter. The waveguides were attached to the actuator by adhering the previously stripped, cleaved, and tapered optical fiber to the piezo bimorphs. It is noteworthy that the heating and pulling method of tapering the optical fiber increases the divergence angle of light projected from the waveguide since the core is modified. In **Figure 1B-1D**, a tapered fiber scanner is photographed at the first three modes of mechanical resonance.

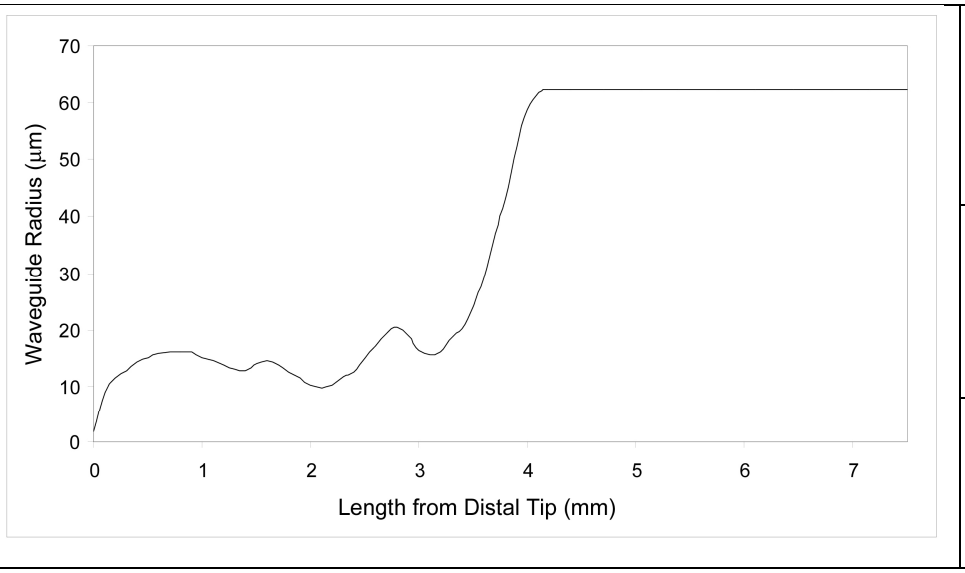

Figure 1: (**A** above left) Radius (microns) versus axial length (mm) of the tapered distal end of a fiber scanner having a complex shape profile from the method of heating and pulling the optical fiber. (**B-C-D** right, top-middle-bottom) First, 2nd , and 3rd modes of mechanical resonance are shown of a tapered fiber, respectively.

A microfabrication method based on acid etching the outer cladding of the optical fiber was used to vary the mass distribution of the fiber scanner while preserving the waveguiding integrity of the core. This method has been discussed previously [7], and is referred to as a three-layer etching process [11] using isooctane, hydrofluoric acid (HF), and Krytox (DuPont Performance Lubricants, Wilmington, DE). The resulting cantilevered optical fiber has a region of reduced diameter where the HF removed the cladding, which is referred to as a notched fiber scanner. Since the core diameter is less than 6 microns on singlemode optical fiber for visible wavelengths, the notch diameter can be as low as 10 microns without affecting the waveguiding properties of the fiber. The notch diameter is controlled by immersion time within the acid etching layer, while the notch length is controlled by the thickness of the acid etching layer. Using machine vision under phase contrast image contrast, real-time control of these parameters can be

accomplished. An example notched fiber is shown at rest and in the first and second mode of mechanical resonance in **Figure 2**.

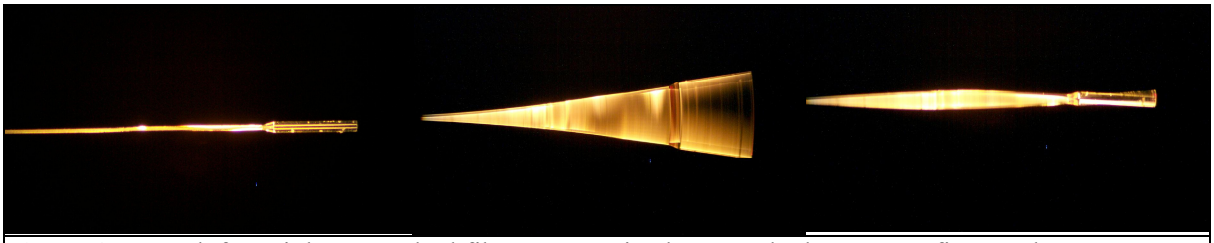

Figure 2: From left to right, a notched fiber scanner is photographed at rest, at first mode resonance (558 Hz), and second mode resonance (6229 Hz). The distal end of the cantilevered notched fiber has the following dimensions: unmodified tip is 990 μm long and 125 μm diameter, notched region is 4.01 mm long and 50 μm diameter, and notch taper lengths are 147 μm near tip & 234 μm near base.

The motion of the fiber scanner was monitored through detection of light projected from the free end of the waveguide using a 635 nm laser diode source (Melles Griot, Inc., Irvine, CA). Light projected from the actuated waveguide was detected using a silicon position-sensing detector (DL-10, UDT Sensors, Inc., Hawthorne, CA) with a surface area of 1 cm^2. Electrical current from the position-sensing detector (PSD) was converted to voltage using standard current-to-voltage circuitry and recorded using a data acquisition card (PCI-6111E, National Instruments, Corp., Austin, TX). The experimental interface and acquisition of data was facilitated by a custom program written in Labview 6i (National Instruments, Corp., Austin, TX). The detector system was calibrated using a three-axis micrometer to move the PSD relative to the free end of the fiber scanner. Voltage measurements recorded from the PSD are linearly related to the position of the light spot on the detector surface. Care was taken to calibrate the detector system for each tested fiber scanner to ensure accurate tip displacement measurement.

In addition to detection of waveguide tip position through use of the PSD, a variable zoom microscope (Edmund Industrial Optics Inc., Barrington, NJ) with an attached CCD camera (XC-75, Sony Corp., New York, NY) was used to take pictures of the actuated fiber scanners during the experiment. Data was acquired from the CCD camera using a frame-capture card (IMAQ PCI-1411, National Instruments Corp, Austin, TX). The CCD-microscope system was calibrated with a precision Ronchi ruling glass slide (Variable Frequency Target, Max Levy Autographic, Philadelphia, PA). Repeated acquisition and measurement of photographs of the Ronchi ruling determined that measurement uncertainty using the microscope was approximately ± 0.7 μm. A tube microscope (NT54-869, Edmund Scientific, Barrington, NJ) with a 10X objective was used to take high magnification pictures of each section of the tapered fiber. These pictures were used to gather dimensional measurements of the tapered fiber shown in **Figure 1A**.

A laser vibrometer system (OFV-2600/OFV-302, Polytec, GmbH., Waldbronn, Germany) was used to measure the motion of the piezo bimorph and piezo stack. The vibrometer is capable of high-speed non-contact measurement of moving surfaces through the use of an interferometric technique. Laser light from the sensor head was focused at a point close to the center of the actuator, near its tip. A lock-in amplifier (SR830 DSP Amplifier, Stanford Research Systems Inc., Sunnyvale, CA) was used to reduce measurement noise of the acquired data. This measurement is useful for determining the base excitation amplitude driving the waveguide vibration.

A sinusoidal voltage was applied to the piezo actuator used to vibrate the fiber scanner. The signal applied to the actuator was generated using the Labview data acquisition program and a GPIB card (PCI-GPIC, National Instruments, Inc., Austin, TX) to trigger a function generator (Model DS345, Stanford Research Systems, Inc., Sunnyvale, CA). The signal output from the function generator was amplified using a high-voltage, high-speed operational amplifier circuit (3584, Burr-Brown, Corp., Tucson, AZ). This configuration of devices allowed for computer control over data acquisition as well as low-noise signal generation at voltages of up to 200V. A diagram that shows each of the devices used in this experiment is shown in **Figure 3**. In experiments using the microfabricated fiber scanners, the bimorph is replaced with a

2 x 3 x 9 mm piezo stack (PICMA Multilayer Piezo Actuator P-882.10, Polytec PI, Inc., Karlsruhe, Germany).

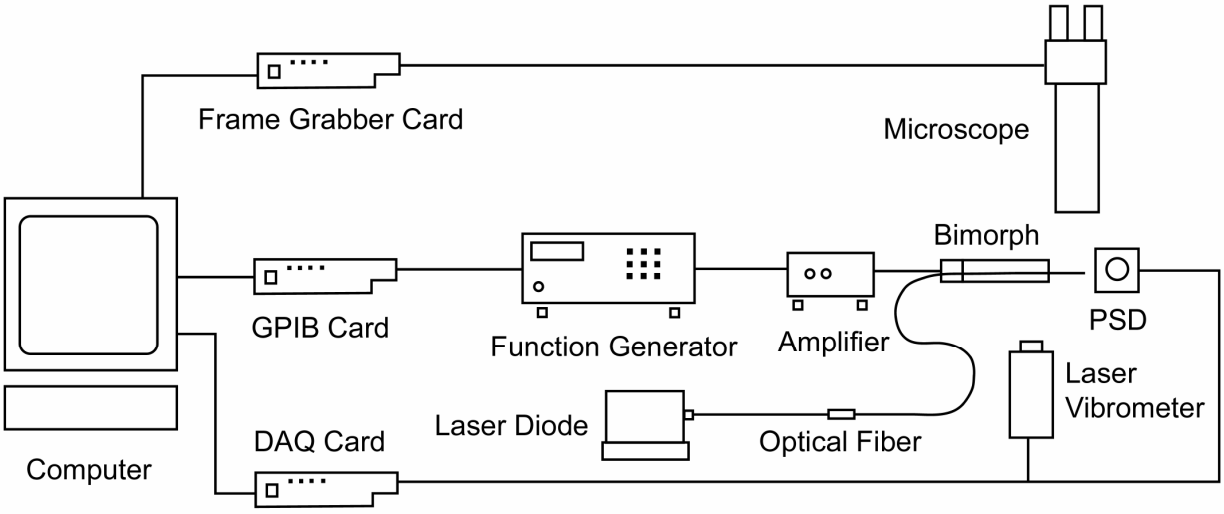

Figure 3: Schematic is shown of the experimental setup for measuring fiber scanner resonant dynamics.

RESULTS

The tapered waveguide was actuated with a range of base excitation magnitudes and frequencies to determine the dynamic response of the system. Recording both the displacement of the bimorph at the waveguide base and the light spot at the PSD allows for the construction of an experimental frequency response function (FRF) as the transfer function (TF), $H(\omega) = T_o/T_i$, where ω is the frequency, T_O denotes light spot displacement at the PSD, and T_i denotes bimorph displacement at the fiber scanner base. It is noteworthy that the experimental setup does not directly measure tip displacement of the waveguide, rather the position of the light spot projected onto the PSD. The PSD is positioned approximately 2.5 mm from the free tip of the waveguide. Comparisons between the FEA model and the experimental results are shown in **Figure 4** for the tapered fiber scanner. The damping coefficient ζ was measured using the half-power bandwidth method by sweeping actuator drive frequency through the lowest three natural frequencies. The resulting damping coefficients are listed in **Table 1** along with comparisons of the experimental versus theoretical resonant frequencies. The FEA model predicted the resonant frequencies of the structure with less than 7% experimental error for each of the first three resonant modes. However, peak amplitudes were predicted with up to 37% error in comparisons for each of the first three resonant modes. The results comparing experimental and theoretical transfer function for all fiber scanners are summarized in **Table 3**.

The error in **Tables 1**, **2**, and **3** is calculated as deviations in percentage from the experimental values. **Table 2** lists the first two resonant frequencies and the damping coefficients measured for the notched fiber scanners and cylindrical fiber scanners (10.2 mm long, 125 μm diameter optical fiber). The FEA models produced less than 10% error for the notched fibers and less than 1% error for the cylindrical fibers. These experimental results differ from the tapered fiber scanner results by the use of a piezo stack actuator for a one-dimensional base translation rather than a piezo bimorph actuator that undergoes a small amount of rotation. In **Table 3**, all fiber scanners and their FEA models are compared to the experimental results with less than 6 % error for cylindrical fiber scanners, while there is 25% error for the notched fiber scanner. Shown in **Figure 5** is a graphical presentation of the comparison between the FEA model and the experimental measurements for the notched fiber scanner. The biggest difference between the notched fiber scanner and other fiber scanner geometries is the measurable TF in the out-of-plane axis (OA) which

is orthogonal to the in-plane axis (IA) defined by the axis of base excitation from the piezo stack. This TF (OA) is almost as high as the TF (IA) in the second resonant mode of the notched fiber scanner.

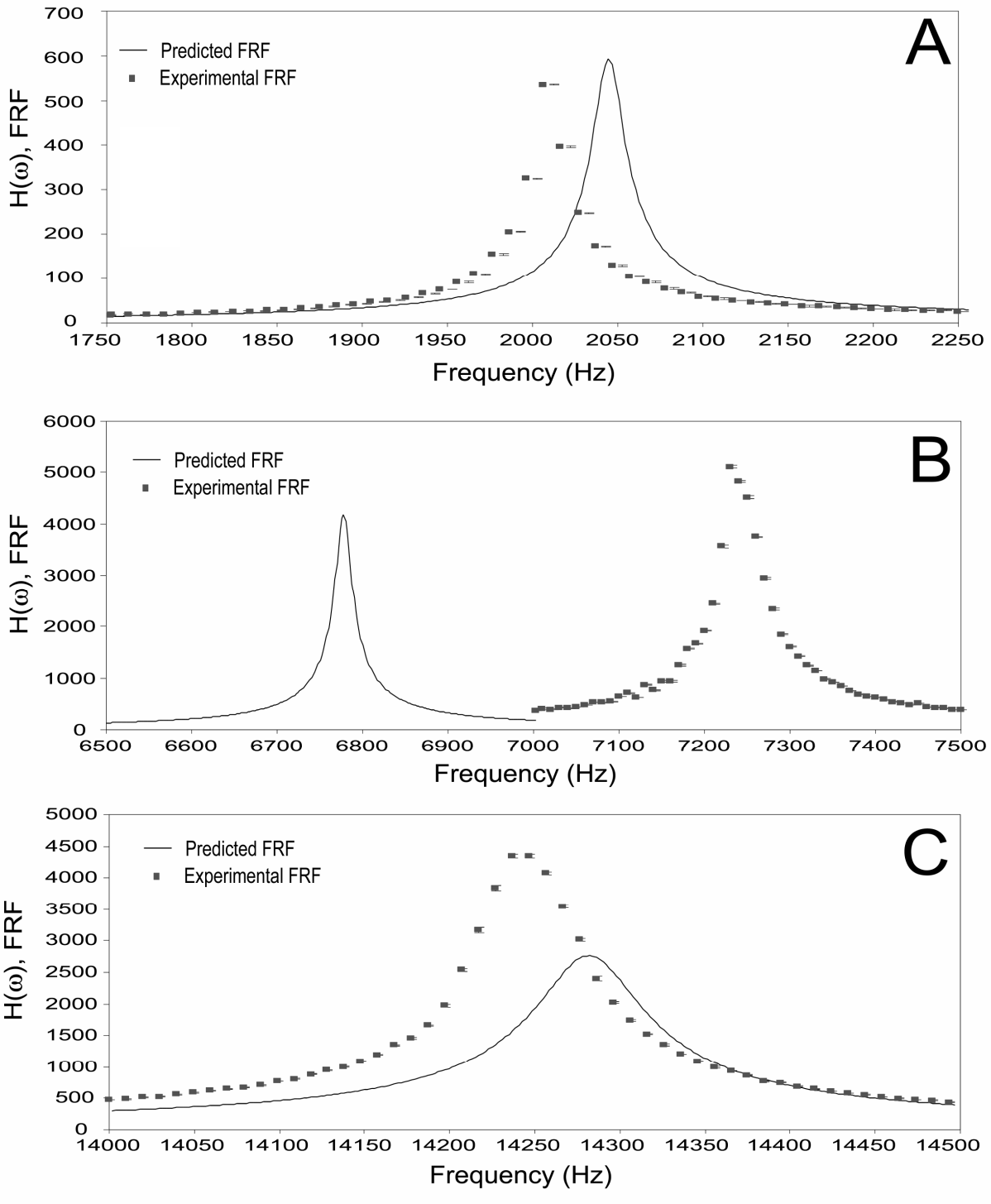

Figure 4: Comparison of experimental and predicted frequency response functions at the first (A), second (B), and third (C) modes of resonance for the tapered fiber scanner with shape profile shown in Figure 1A.

Table 1: Experimentally determined resonant frequencies, damping coefficients, and comparison to the theoretical FEA model of the tapered fiber scanner with complex profile shown in Figure 1A.				
Fiber scanner profile and resonant mode	Experimental resonant freq. [KHz]	Experimental damping coef. [ζ]	Theoretical resonant freq. [Hz]	Error [%]
Tapered (1st)	2.010	0.0045	2.040	1.5
Tapered (2nd)	7.260	0.0014	6.774	6.7
Tapered (3rd)	14.240	0.0022	14.288	0.3

Table 2: Experimentally determined resonant frequencies, damping coefficients, and the comparison to the theoretical FEA models of the cylindrical and microfabricated fiber scanner described in Figure 2.				
Fiber scanner profile and resonant mode	Experimental resonant freq. [Hz]	Experimental damping coef. [ζ]	Theoretical resonant freq. [Hz]	Error [%]
Cylindrical (1st)	966	0.0015	968	0.21
Cylindrical (2nd)	6058	0.00083	6063	0.08
Notched (1st)	628	0.00159	682	8.60
Notched (2nd)	6631	0.00098	7082	6.80

Table 3: Comparison of fiber scanners with tapered, cylindrical, and notched geometries and their experimental maximum amplitude in terms of transfer function compared to theoretical FEA models.			
Fiber scanner profile and resonant mode	Experimental Transfer Function (TF)	Theoretical Transfer Function (TF)	Error (%)
Tapered (1st)	535	593	10.8
Tapered (2nd)	5107	4147	18.8
Tapered (3rd)	4388	2761	37.1
Cylindrical (1st)	680	640	5.9
Cylindrical (2nd)	1041	1013	2.7
Notched (1st)	620	593	4.4
Notched (2nd)	1148	859	25.2

The FEA model of the notched fiber scanner is used to select the preferred fiber scanner design of highest TF of tip displacement or deflection angle while maintaining highest resonant frequency. A notch of 1 mm in length and 40 microns in diameter was modeled at various positions from being centered at 1 mm from the base to 1 mm from the tip of a 10 mm long cantilever, and results are shown in **Figures 6** and **7**. Important note of comparison is between the results for the cylindrical fiber scanner in **Tables 2** and **3** and the notched fiber designs selected from **Figures 6** and **7**. For first mode resonance, the selected scanner design from **Figure 6** is a notch centered at 7.5 mm from the base which has a transfer function of 900 compared to less than 700 for the cylindrical fiber scanner, while both designs are resonant at about 1000 Hz. For the second mode resonance, the selected scanner design from **Figure 7** is a notch centered at 8.5 mm from the base which has a TF of 2000 and resonance at 5 KHz compared to the cylindrical fiber scanner having a TF of less than 1100 and a resonance frequency at 6 KHz.

Using a finite differencing technique, the nonlinear behavior of fiber scanners can be modeled. Preliminary transfer function results are shown in **Figures 8** about the first resonance frequency with base excitation being a sinusoid along the in-plane direction at three microns peak-to-peak. Although not excited in the out-of-plane axis, the nonlinear bending term provides cross-coupling from the in-plane axis to the out-of-plane axis. The result at higher base excitations (above 0.1 microns) produces tip displacement in the out-of-plane direction, amplitude jump, and whirl, transforming a 1D response to a 2D response as shown in **Figures 8**. In addition, the first-mode frequency plots demonstrate a softening spring nonlinear response, meaning the amplitude peak is bending towards the lower frequencies as though the

spring coefficient is becoming softer with increasing tip displacements. In comparison to the analytical results of Smithwick et al., [12] for a straight cylindrical cantilever, these results match qualitatively the predicted softening spring nonlinear response for first mode, and a hardening spring nonlinear response for the second mode of resonance (not shown). However, unlike the analytical results of the simple geometry in Smithwick et al., these complex shapes of tapered fiber scanners and three-layer etched or notched fiber scanners can be modeled more easily for future design optimization using finite differencing or finite element analyses.

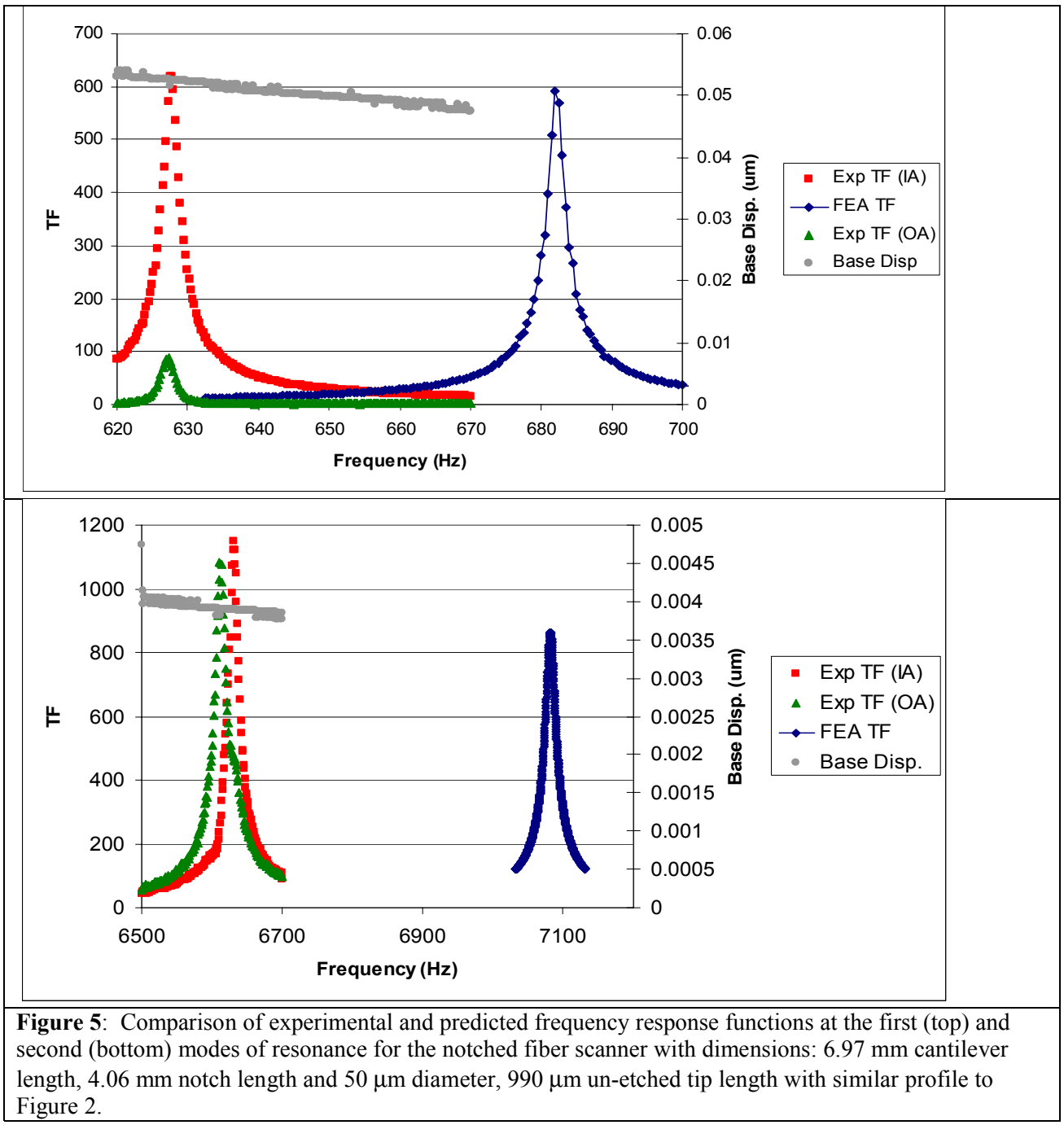

Figure 5: Comparison of experimental and predicted frequency response functions at the first (top) and second (bottom) modes of resonance for the notched fiber scanner with dimensions: 6.97 mm cantilever length, 4.06 mm notch length and 50 µm diameter, 990 µm un-etched tip length with similar profile to Figure 2.

A

B

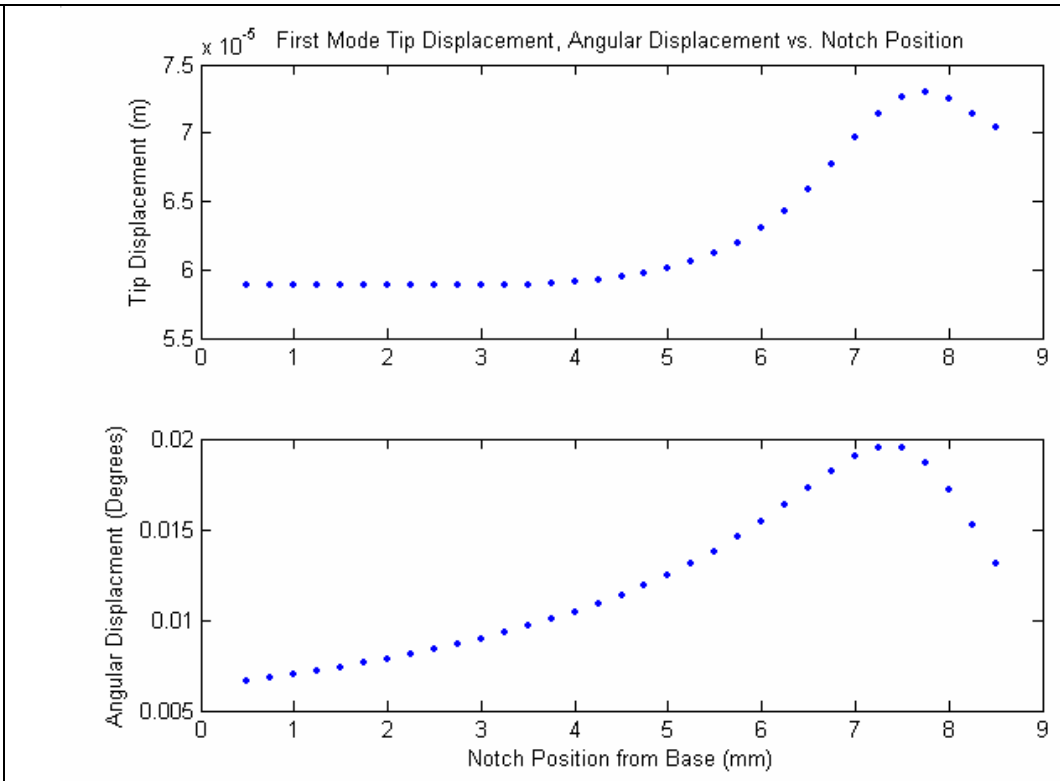

C

D

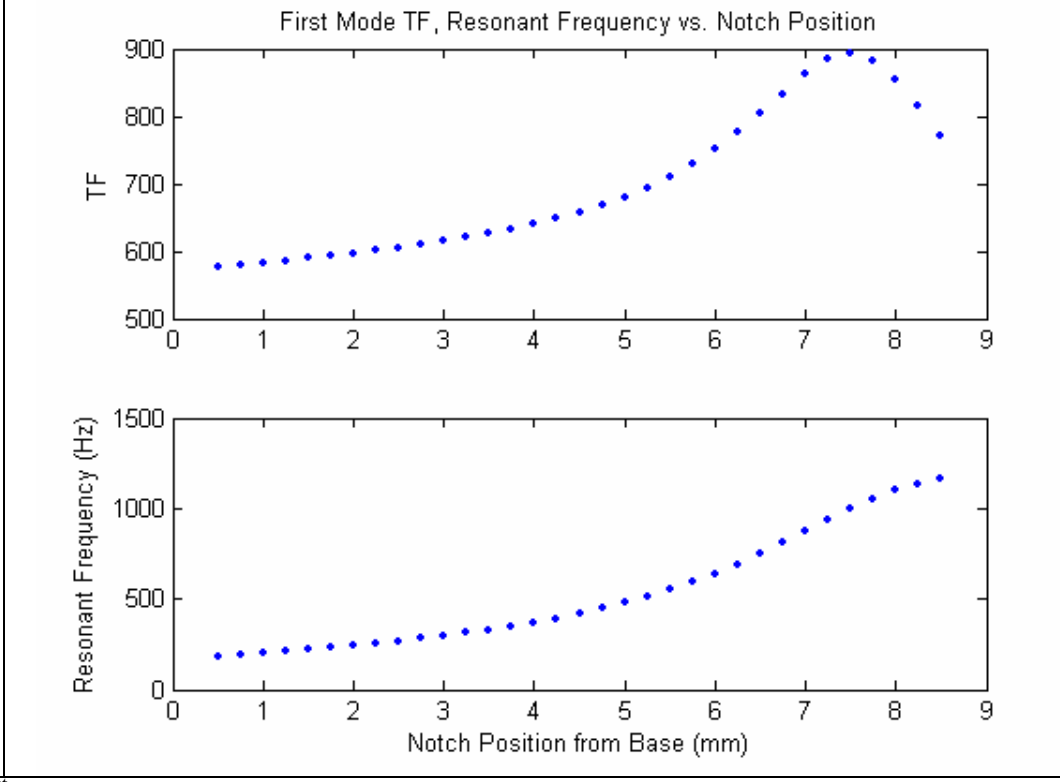

Figure 6: 1st mode FEA modeling results varying the 1 mm long and 40 micron diameter notch location. A is Tip displacement, B is Tip deflection angle, C is Transfer Function, and D is Resonant frequency.

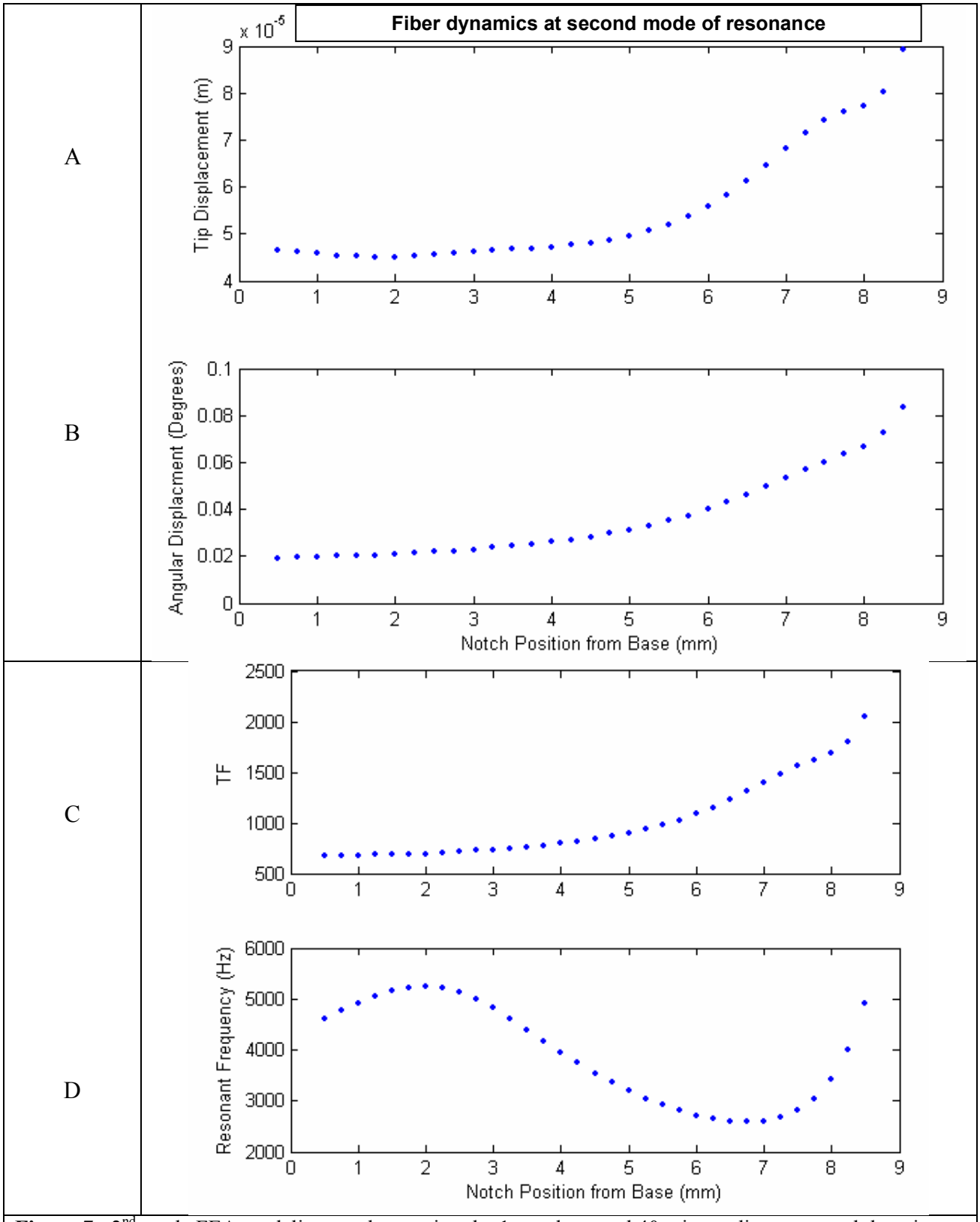

Figure 7: 2nd mode FEA modeling results varying the 1 mm long and 40 micron diameter notch location. A is Tip displacement, B is Tip deflection angle, C is Transfer Function, and D is Resonant frequency.

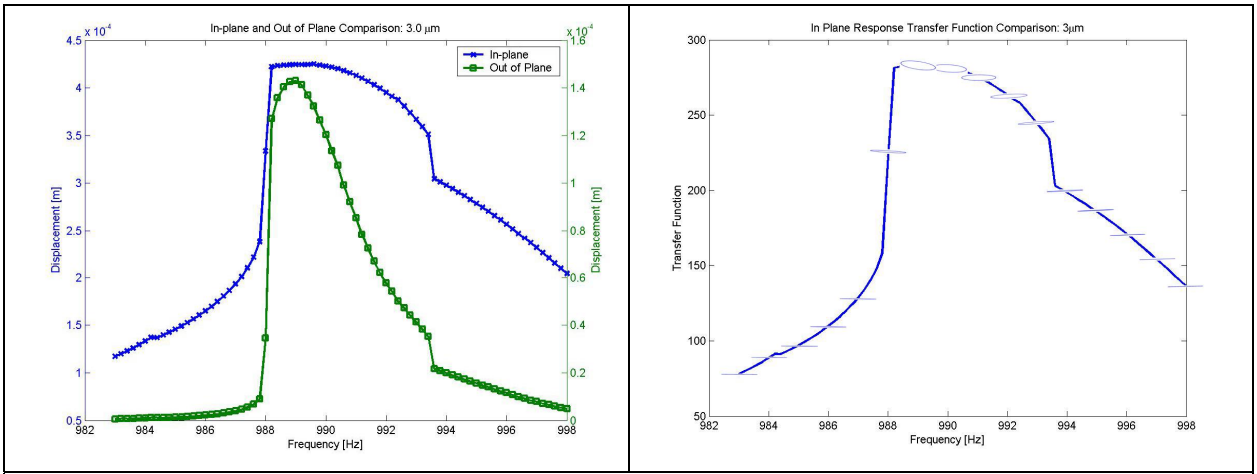

Figure 8: (left) Nonlinear dynamics of the cylindrical fiber scanner are plotted in terms of the in-plane and out-of-plane response with respect to linear 3μm base displacement. (right) Transfer function (TF) of the in-plane response is plotted with points indicating the percentage of out-of-plane response in each region of the curve, (a circle would indicate that in-plane and out-of-plane responses are of equal magnitude).

DISCUSSION & CONCLUSIONS

The FEA model of the cylindrical fiber scanner matched experimental results in both frequency and amplitude of the first two modes of resonance to less than 10% error. Three to four times this error was observed in comparisons between FEA models of fiber scanners exhibiting the complex shape profiles of tapered and notched cantilevers. The FEA models rely on many assumptions, such as isotropic material properties that do not change after the microfabrication process. Geometrically, the assumption of axial symmetry is applied to all FEA models, but observed not to be true for many of the heated and pulled (tapered) fibers. The experimental means of base excitation was changed from a piezo bimorph to a piezo stack actuator to better match the FEA model assumption of fiber base displacement along one axis. Thus the tapered fiber scanner results may have artificially high TF in **Table 3** compared to the more accurate model predictions of cylindrical and notched fiber scanners. Finally, the FEA models are limited to the condition of only small base excitation, the linear in-plane response of the dynamic system.

Although limited in absolute accuracy, the FEA models of fiber scanners can be useful as a mechanism to choose between designs based on their relative performance within the linear regime, while assuming that 1D resonance extrapolates to 2D. By selectively removing cladding mass along the fiber scanner, the frequency and amplitude of the resonance can be manipulated. By sweeping a fixed notch size from the base to the tip of the fiber scanner, the best design that combines high amplitude (wide FOV or greatest efficiency) while maintaining high resonance frequency can be identified. For first mode of resonance, the selected notched fiber scanner design produces a transfer function 30% greater than the unmodified cylindrical fiber scanner without sacrificing any frequency. The notched fiber scanner design selected for the second mode resonance produces almost twice the maximum TF while sacrificing less than 20% of the resonance frequency. Interestingly, the preferred notch location is adjacent to the free end of the fiber scanner, leaving a short length of un-etched fiber at the distal tip for a future microlens as previously proposed [11]. These preliminary results from FEA modeling support our hypothesis that complex mass distribution along the fiber scanner axis can improve scanner efficiency.

The experimentally measured damping coefficient of each resonant frequency of the fiber scanner can have significant effects on the amplitude of the simulated response. Research is ongoing to evaluate damping of the fiber scanner and create a theoretical model of the damping as a function of material and design parameters. At this point in modeling the fiber scanner with the inclusion of the nonlinear curvature

term only, the presence of amplitude jump and whirl are quite evident. Furthermore, we see significant out of plane motion at resonance that, as expected, disappears when the actuation frequency is away from the resonant frequency of the fiber scanner. Inclusion of other nonlinear terms, such as nonlinear inertia, is expected to increase the accuracy of the model. Future models will also include the effects of slight rotation at the fiber base from the use of bending piezo actuators and nonsymmetrical cross sections of the fiber. The predictive value of these models will be verified by directing the fabrication of fiber scanners which require less electrical power to drive the fiber resonance and/or reducing the rigid length of the distal tip.

ACKNOWLEDGEMENT

Conception and first demonstration of three-layer etching and testing of fiber scanners are by Mark Fauver. Notched fiber scanners are made by Satoshi Karasawa in the Human Interface Technology Laboratory. Funding for this work is from the NIH/NCI grant CA094303 and the Pentax Corporation, Tokyo, Japan.

REFERENCES

[1] Seibel, E.J., Smithwick, Q.Y.J., Brown, C.M., Reinhall, P.G., 2001, Single fiber flexible endoscope: general design for small size, high resolution, and wide field of view, **Biomonitoring and Endoscopy Technologies**, Proc. SPIE, 4158, 29-39.

[2] Seibel, E.J., and Smithwick, Q.Y.J., (2002), Unique features of optical scanning, single fiber endoscopy, **Lasers in Surgery and Medicine**, 30, 177-183.

[3] Wang, J., and Langer, S., (1997), Brief review of human perception factors in digital displays for picture archiving and communications systems, **Journal of Digital Imaging**, 10(4), 158-168.

[4] Bryant, R.C., Seibel, E.J., Lee, C.M., and Schroder, K.E. (2004) Low-cost wearable low-vision aid using a handmade retinal light-scanning microdisplay. **Journal of the SID**, 12(4): 397-404.

[5] Johnston, R.S. and Seibel, E.J. (2004) Scanning fiber endoscope prototype performance, **Frontiers in Optics 2004**, Optical Society of America, October 10-14, 2004, Rochester, NY. Technical Digest ñ Paper FWM2.

[6] Yang, Y.T., Heh, D., Wei, P.K., and Fann, W.S., 1997, Vibration dynamics of tapered optical fiber probes, **J. Appl. Phys**. 81, 1623-1627.

[7] Fauver, M., Crossman-Bosworth, J., and Seibel, E.J. (2002) Microfabrication of fiber optic scanners. **Optical Scanning 2002**, Proc. SPIE vol. 4733:102-110.

[8] R.A. Paquin, **Optomechanical Engineering Handbook**, (1999), CRC Press, Boca Raton, FL.

[9] Kundrat, Matthew J. (2004) A nonlinear numerical model of a base excited cantilever beam. **Masters Thesis,** Mechanical Engineering, University of Washington, Seattle, WA.

[10] Pai, P.F. and Nayfeh, A.H. (1990) Non-linear non-planar oscillations of a cantilever beam under lateral base excitations. **Intl. J. Non-linear Mechanics**, 25(5): 455-474.

[11] Seibel, E.J., Fauver, M., Crossman-Bosworth, J., Smithwick, Q.Y.J., and Brown, C.M. (2003) Microfabricated optical fiber with microlens that produces large field-of-view, video rate, optical beam scanning for microendoscopy applications. **Optical Fibers and Sensors for Medical Applications III**, Proc. SPIE, 4957: 46-55.

[12] Smithwick, Q.Y.J., Reinhall, P.G., Vagners, J., Seibel, E.J. (2004) A nonlinear state-space model of the resonating single fiber scanner for tracking control: theory and experiment. **ASME Journal of Dynamic Systems, Measurement, and Control,** vol. 126: 88-101.